

# Model Predictive Pulse Pattern Control for Modular Multilevel Converters

Michail Vasiladiotis, *Member, IEEE*, Alexandre Christe, *Student Member, IEEE*,  
and Tobias Geyer, *Senior Member, IEEE*

**Abstract**—For dc/ac modular multilevel converters (MMCs) in double-star configuration, this paper proposes a fast closed-loop control method based on optimized pulse patterns (OPPs). Thanks to the direct manipulation of the OPP switching instants, OPPs with discontinuous switching angles can be used, and the intrinsic cell capacitor voltage ripple is compensated for to preserve the OPPs' superior harmonic performance. This model predictive pulse pattern controller (MP<sup>3</sup>C) is combined with a fast acting dead-beat circulating current controller (DBC<sup>3</sup>) and linked to an upper layer voltage balancing control scheme. The proposed control and modulation method is particularly suitable for medium voltage MMCs with a low number of cells. Despite operation at very low switching frequencies close to and including the fundamental frequency, a superior harmonic performance can be achieved.

**Index Terms**—Circulating current control, dead-beat control, harmonics, model predictive control, modular multilevel converter, modulation, optimized pulse pattern.

## I. INTRODUCTION

THE modular multilevel converter (MMC) exhibits several attractive features for applications that require high voltages and high power. These include straightforward voltage and power scalability, very low harmonic emission, high availability as well as fault tolerance [1], [2]. On the other hand, medium voltage dc/ac MMCs are emerging in solar, dc grid, battery energy storage systems and variable speed drives. These applications are characterized by relatively low power ratings, which implies that only a few cells are needed, especially if high-voltage low-loss semiconductors are used. In order to maximize the converter efficiency, as low a semiconductor switching frequency as possible is chosen. This leads to a low number of voltage levels and a low apparent switching frequency at the converter phase terminals, which results in an inferior harmonic performance of the converter. Eventually, a filter on the three-phase side might be needed, in order to meet the grid-side harmonic requirements. In this case, a modulation method that allows the shaping of the harmonic spectrum is preferred to minimize the filter size.

Manuscript received September 15, 2017; revised March 23, 2018; accepted August 17, 2018.

Michail Vasiladiotis is with ABB Switzerland Ltd, 5300 Turgi, Switzerland (e-mail: michail.vasiladiotis@ch.abb.com.)

Alexandre Christe is with ABB Corporate Research, 722 26 Västerås, Sweden (e-mail: alexandre.christe@se.abb.com.)

Tobias Geyer is with ABB Corporate Research, 5405 Baden-Dättwil, Switzerland (e-mail: t.geyer@ieee.org.)

For these emerging MMC applications, the aforementioned shortcomings of the state-of-the-art methods necessitate the use of more advanced modulation concepts, such as optimized pulse patterns (OPPs) [3]. However, OPPs cannot be easily combined with a closed-loop control system for several reasons. First, discontinuities in the switching angles when varying the modulation index prevent the use of linear controllers due to stability issues. Second, unlike modulation methods with a fixed modulation cycle such as carrier-based pulse width modulation (CB-PWM) and space vector modulation (SVM), OPPs are associated with a non-zero ripple current at the end of the switching period. The bandwidth of a conventional current controller thus has to be slow, limiting the capability of the controller to reject disturbances and to react to transients. Last but not least, OPPs are typically calculated considering ideal conditions, i.e., neglecting system disturbances. The considerable inherent capacitor voltage ripples and other system non-idealities prevent the use of OPPs for MMCs without fast control loops.

The use of selective harmonic elimination (SHE) and OPPs with continuous angles has been investigated in the literature for the dc/ac MMC in double-star configuration [4]–[11]. Specifically, [5] and [6] present the design and application of the patterns directly on the level of the converter branches. In addition, only fundamental switching frequency is discussed, which significantly limits the flexibility for shaping the harmonic spectrum. On the contrary, the authors of [7] design the SHE pattern directly on the level of the three-phase side voltage. The results are then mapped to branch-level command signals for the upper and lower branches of the same converter phase-leg. In all of the above cases, either no controller or a very slow linear controller were used. In addition, the ripple on the capacitor voltages was ignored, which means that the pre-calculated switching patterns are applied in an open-loop fashion, forgoing optimality. Reference [5] also discusses circulating current control for the  $(N + 1)$ -level-modulated dc/ac MMC in double-star configuration. The latter has very slow dynamics and is used to compensate only the even harmonics in the circulating current; the odd harmonics are left uncontrolled to achieve vertical self-balancing. In addition, the circulating current control acts as a standalone function and no interface with a global MMC inner branch capacitor voltage control layer is discussed. Circulating current control for a  $(2N + 1)$ -level-modulated dc/ac MMC in double-star configuration is discussed in [8].

Contrary to the above mentioned literature, this paper

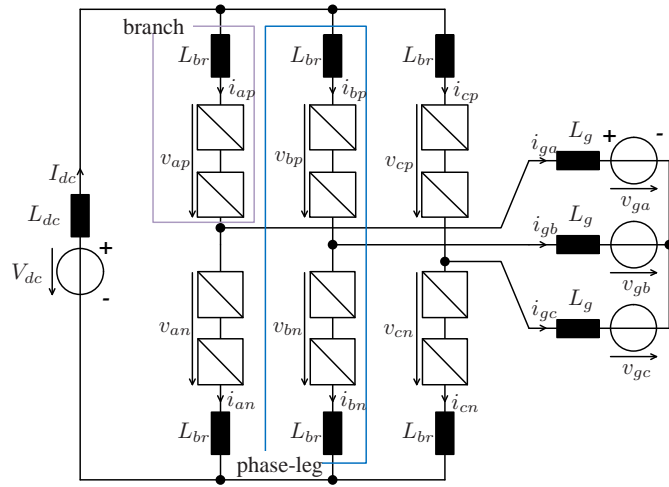


Fig. 1. The three-phase dc/ac MMC in double-star configuration.

proposes a *fast* closed-loop control scheme for three-phase dc/ac MMCs in double-star configuration using OPPs with *discontinuous* switching angles. The proposed controller is based on the model predictive pulse pattern control (MP<sup>3</sup>C) concept [12]. MP<sup>3</sup>C modifies the OPP switching instants in the converter branches in a receding horizon fashion. For the MMC, fast closed-loop control via the switching instants compensates for various system disturbances, such as the cell capacitor voltage ripples, which would otherwise impair optimality of the pre-calculated pulse patterns. It is noted that MP<sup>3</sup>C was applied successfully to a static synchronous compensator (STATCOM) based on a delta-connected MMC [13], as well as to a railway inertia based on a direct ac/ac MMC by utilizing a decoupled modulation concept [14].

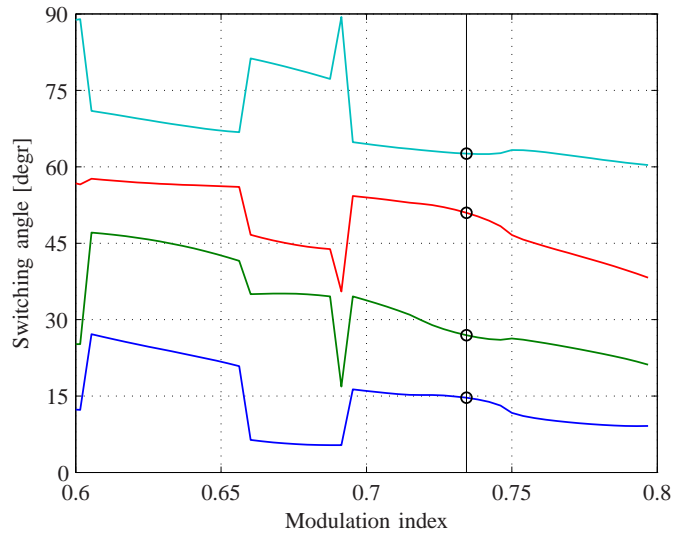
This paper augments MP<sup>3</sup>C to enable circulating current control for three-phase dc/ac MMCs in double-star configuration. Specifically for  $N + 1$  modulation, a high-bandwidth dead-beat circulating current controller (DBC<sup>3</sup>) is proposed, which offers significantly improved dynamics at low switching frequencies compared to previous works, which lacked a circulating current controller [7] or reported a very slow control method [5]. Finally, the appropriate interface of the proposed methods to the superimposed MMC voltage balancing controllers is analyzed.

The outline is as follows: Section II provides the basics about the dc/ac MMC, OPPs as well as the MP<sup>3</sup>C concept. Section III provides an in-depth analysis of the combined MP<sup>3</sup>C and circulating current control as well as their integration into the global control scheme. Section IV evaluates the transient and harmonic performance of the proposed method. Finally, Section V concludes the work.

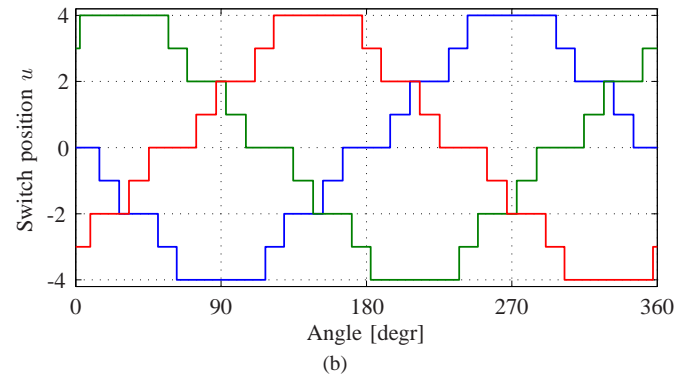
## II. MP<sup>3</sup>C FOR DOUBLE STAR-CONFIGURED MMC

### A. MMC topology and modulation

The MMC consists of series-connected cells (which are also known as modules or submodules), forming what is called a converter branch (or arm). These branches can be configured in several ways, leading to dedicated converter topologies. Depending on whether this branch needs to provide only



(a)



(b)

Fig. 2. Discontinuous three-phase OPP for an MMC with  $N = 8$  cells per branch,  $N + 1$  modulation (9-level) and operation at fundamental switching frequency ( $d = 4$ ): (a) switching angles for a certain range of modulation indices and (b) three-phase voltage pattern over  $[0, 360]$  degrees for one particular modulation index, which is highlighted by the vertical line in (a).

positive or also negative voltages, the cell can be implemented as unipolar or bipolar type, respectively.

The considered dc/ac MMC topology in double-star configuration is depicted in Fig. 1. It connects a medium voltage dc line (or network) to a three-phase grid. The circulating currents in the phase-legs can be used as a degree of freedom to balance between the branches the energy stored in the capacitors.

It is widely known from the literature that two types of modulation methods can be applied to the double star-configured dc/ac MMC. They are tightly linked to the number of levels in the phase voltage waveform and influence the way the circulating current control can be performed.

1)  $N + 1$  modulation: Both the upper and lower branches of the same phase-leg are switched synchronously in opposite direction when a switching event in the phase voltage pattern occurs. The sum of the inserted cells per phase-leg, when no circulating current control is applied, is equal to  $N$ . Therefore, the expression  $n_{up} + n_{low} = N$  holds, where  $N$  is the number of cells per branch and  $n_{up}$  ( $n_{low}$ ) denotes the number of modules inserted into the upper (lower) branch.

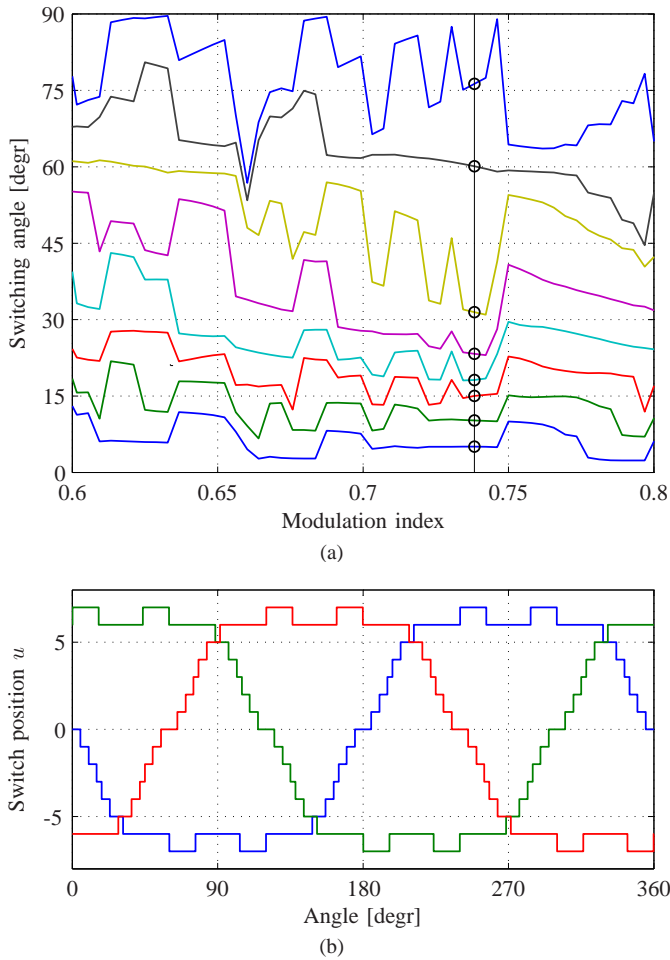


Fig. 3. Discontinuous three-phase OPP for an MMC with  $N = 8$  cells per branch,  $2N + 1$  modulation (17-level) and operation at fundamental switching frequency ( $d = 8$ ): (a) switching angles for a certain range of modulation indices and (b) three-phase voltage pattern over  $[0, 360]$  degrees for one particular modulation index highlighted by the vertical line in (a).

2)  $2N + 1$  modulation: Only one of the two branches is switched when a switching event occurs in the phase voltage pattern. The upper and lower branches are switched asynchronously and—as a consequence—the sum of the inserted modules per phase-leg is not always equal to  $N$ , but can take three values:  $n_{up} + n_{low} \in \{N - 1, N, N + 1\}$ , if only a minimum deviation between  $N - n_{up}$  and  $n_{low}$  is considered. As a result, the number of phase voltage levels is almost doubled for the same semiconductor switching frequency.

### B. OPPs for MMCs

OPP are calculated by minimizing a cost function related to the total demand distortion (TDD) of the desired voltage or current waveform. Additional constraints, e.g., the minimization of specific harmonics can be added to the optimization problem. Figure 2 shows the result of an optimization procedure for a three-phase MMC with  $N = 8$  cells per branch operating at fundamental switching frequency. This implies an OPP with  $d = 4$  switching transitions within a quarter of the fundamental period. It is noted that such quarter-

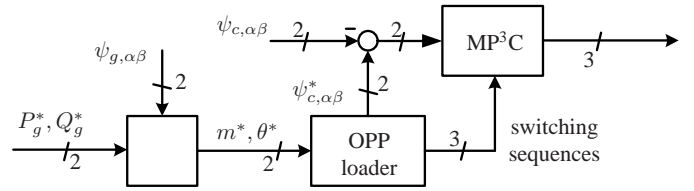


Fig. 4. The general MP3C principle [12].

wave symmetry ensures the absence of even harmonics in the resulting voltage spectrum. The highly discontinuous nature of the OPP's switching angles is also evident.

Consider the same converter with the same number of cells operating at the same semiconductor switching frequency. When operating with  $2N + 1$  modulation, an OPP with twice as many switching angles (here  $d = 8$ ) and twice as many voltage levels (here 17) has to be computed. An example of such an OPP is shown in Fig. 3.

### C. Closed-loop pulse pattern control concept

The proposed closed-loop pulse pattern control concept for the dc/ac MMC is illustrated in Fig. 4. Given the average active and reactive power references  $P_g^*$  and  $Q_g^*$ , the estimate of the virtual grid flux vector  $\psi_{g,\alpha\beta} = [\psi_{g\alpha} \ \psi_{g\beta}]^T$  and the equivalent grid inductance  $L_{g,eq} = L_{br}/2 + L_g$ , the ideal converter flux reference  $\bar{\psi}_{c,\alpha\beta}^* = [\bar{\psi}_{c\alpha}^* \ \bar{\psi}_{c\beta}^*]^T$  is determined. This is typically done in the stationary orthogonal reference frame using

$$\begin{bmatrix} \bar{\psi}_{c\alpha}^* \\ \bar{\psi}_{c\beta}^* \end{bmatrix} = \begin{bmatrix} \psi_{g\alpha} \\ \psi_{g\beta} \end{bmatrix} + \frac{2}{3} \frac{L_{g,eq}}{\omega_g (\psi_{g\alpha}^2 + \psi_{g\beta}^2)} \begin{bmatrix} -\psi_{g\beta} & \psi_{g\alpha} \\ \psi_{g\alpha} & \psi_{g\beta} \end{bmatrix} \begin{bmatrix} P_g^* \\ Q_g^* \end{bmatrix}, \quad (1)$$

where  $\omega_g$  denotes the angular grid frequency.

The magnitude of the converter flux reference is translated into a desired modulation index  $m^*$ . If the desired modulation index differs by a certain threshold from the actual modulation index, a (new) OPP is loaded with the desired pulse number  $d$ . The integral of the switched voltage waveform constitutes the reference trajectory of the virtual converter flux. The ideal converter flux reference is then mapped into the corresponding reference point  $\psi_{c,\alpha\beta}^*$  on the reference trajectory. Note that the reference trajectory includes the switching ripple, whereas the ideal converter flux reference neglects it. Therefore, in general,  $\psi_{c,\alpha\beta}^*$  differs from  $\bar{\psi}_{c,\alpha\beta}^*$ .

The controller forces the virtual converter flux  $\psi_{c,\alpha\beta}$  to track the OPP flux trajectory. To achieve this, the controller minimizes the flux error in the stationary reference frame

$$\psi_{e,\alpha\beta} = \psi_{c,\alpha\beta}^* - \psi_{c,\alpha\beta} \quad (2)$$

by modifying the switching instants of the OPP. In the simplest case, a dead-beat (DB) controller can be used in  $abc$ -coordinates. This leads to the  $abc$ -correction times

$$\Delta t = \frac{\psi_e}{-\Delta u V_{lvl}} \quad (3)$$

where  $\psi_e$  denotes the flux error in  $abc$ -coordinates,  $\Delta u = u_i - u_{i-1}$  denotes the change in the switch position of the switching sequence and  $V_{lvl}$  corresponds to the voltage step in the phase voltage waveform.

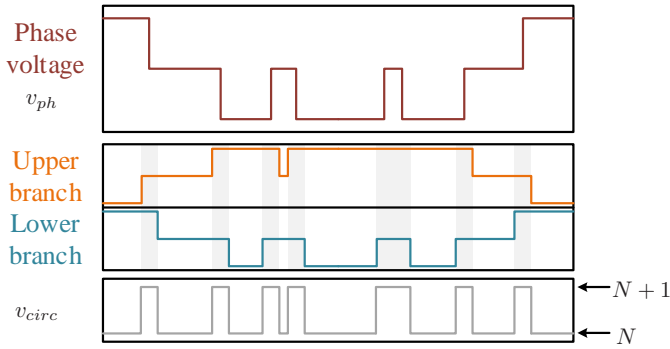


Fig. 5.  $N + 1$  modulation: Circulating current control by inserting redundant levels (in this case, an  $N + 1$  redundant level is inserted).

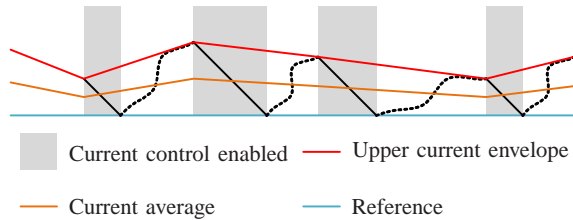


Fig. 6. Dead-beat circulating current controller (DBC<sup>3</sup>) behavior for the  $N + 1$  modulation case.

This pulse pattern control method is also referred to as model predictive pulse pattern control (MP<sup>3</sup>C) [12]. The flux error is minimized over a prediction horizon by computing a modified switching sequence. Only the first part of the switching sequence within the time interval  $[t, t + T_s]$  is applied to the converter, where  $T_s$  denotes the sampling interval. At the next sampling instant, using new measurements (or estimates), the flux error minimization procedure is repeated over a shifted or receding prediction horizon. This so-called receding horizon policy provides feedback and ensures that the controller is robust to parameter uncertainties. The prediction horizon is required to be sufficiently long to include at least two switching events in two different phases. This ensures that the controller can drive (small) flux errors to zero within the horizon.

Several constraints are added to the control problem: (a) a switching transition cannot be moved into the past (or before the current sampling instant), and (b) a switching transition cannot be moved before or after another switching transition in the same phase. It is noted that the control algorithm is computationally efficient and requires only a few microseconds of computation time on a standard control hardware system.

Such a three-phase control and modulation approach is beneficial for switching frequency reduction, as any of the three phases can be used for flux error correction without the need for additional switching events. This is in contrast to single-phase modulation concepts. Furthermore, thanks to the dead-beat control behavior of the pattern controller, very fast current and power responses can be achieved during transients.

### III. MMC INNER CONTROL

Circulating current control can be achieved through the timing and/or insertion of so-called redundant levels [8].

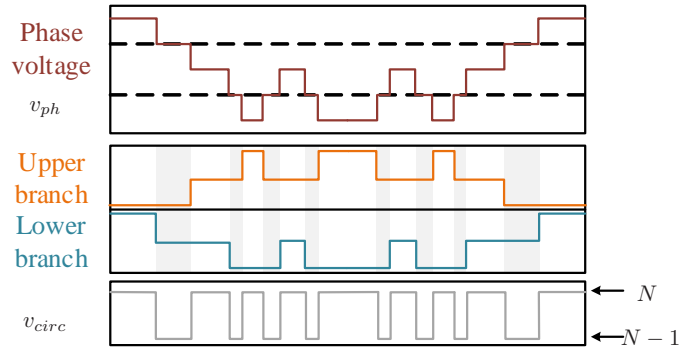


Fig. 7.  $2N + 1$  modulation: Circulating current control by selecting redundant levels (in this case, an  $N - 1$  redundant level is selected).

Redundant levels arise when the number of inserted cells in the upper and the lower branches does not sum up to  $N$ . The closest neighbors are  $N + 1$  and  $N - 1$ , and they can be applied without increasing the semiconductor switching frequency. It is noted that redundant levels with  $N - x / N + x$  and  $x > 1$  are also possible by inserting pulses at the expense of an increased switching frequency.

#### A. Circulating current control with $N + 1$ modulation

With  $N + 1$  modulation, the redundant levels have to be actively inserted by advancing or delaying switching transitions in a symmetrical manner between the upper and lower branches [5]. A symmetrical correction reduces the negative impact on the three-phase converter flux. An example of this mechanism is illustrated in Fig. 5. The circulating current control for  $N + 1$  modulation can be added in a straightforward manner to the existing virtual grid flux MP<sup>3</sup>C control. More specifically, the circulating current error is translated into a correction time that is applied in an opposite manner (with different signs) to the upper and lower branches of the same phase-leg. The correction time is calculated as

$$\Delta t_{corr} = -2L_{br} \frac{\Delta i_{circ}}{V_{lv}} \quad (4)$$

This control principle is event-based, i.e., the circulating current controller is effective only in the vicinity of the switching transitions, as illustrated in Fig. 6.

#### B. Circulating current control with $2N + 1$ modulation

With  $2N + 1$  modulation, the redundant levels are present by default and the only degree of freedom is their selection (either  $N + 1$  or  $N - 1$ ), but not their duration. This strongly affects the way the circulating current can be controlled and the achievable control performance. An example of this mechanism is illustrated in Fig. 7. The  $2N + 1$  modulation requires a switching event distribution logic, which selects between the  $N + 1$  and  $N - 1$  redundant levels, akin to a hysteresis controller as indicated in [8]. More specifically, the controller acts on the sign of the circulating current error  $i_{circ, err} = i_{circ}^* - i_{circ}$ .

For a low number of cells per branch, the circulating current features a strong ripple at the apparent switching frequency.

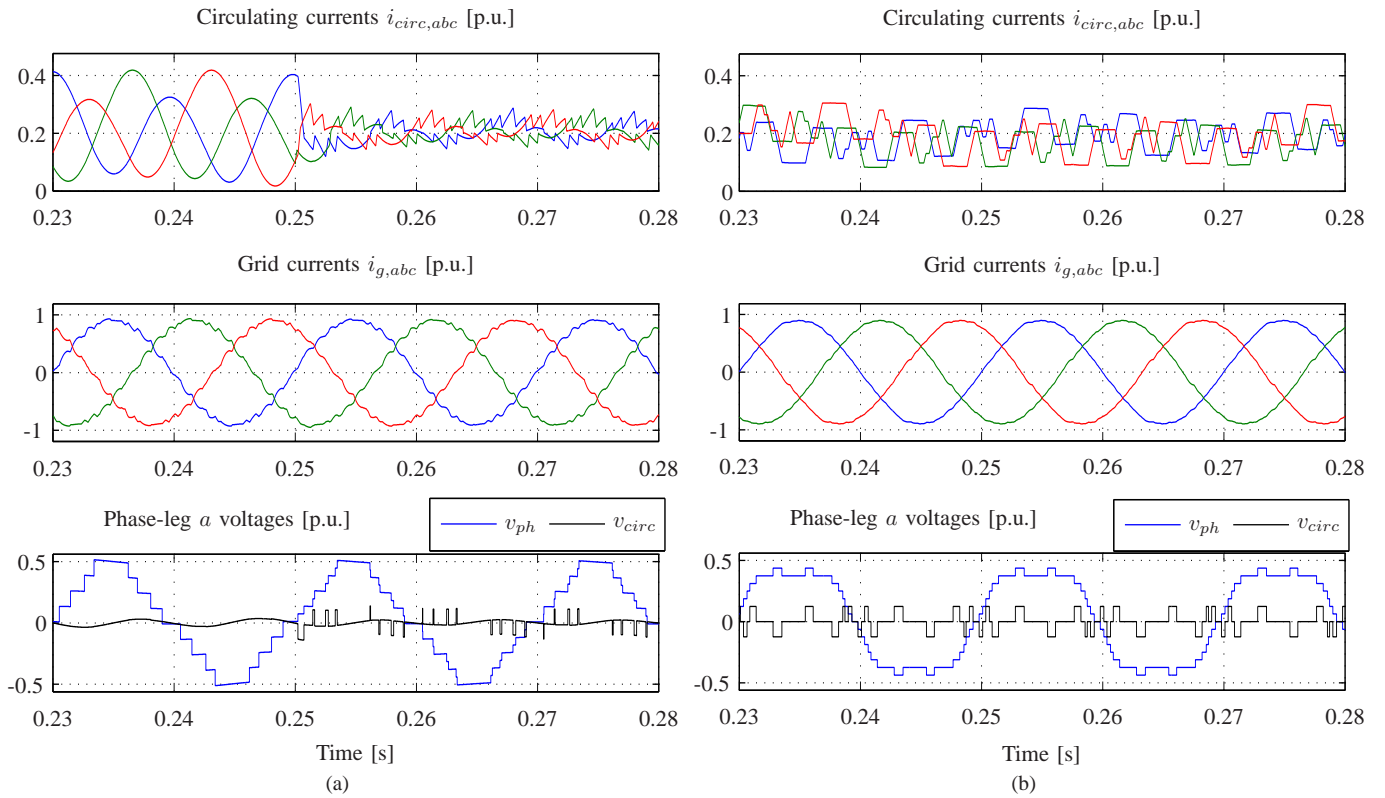


Fig. 8. Simulation results for the circulating current control in MP<sup>3</sup>C-controlled dc/ac MMC in double-star configuration: (a)  $N + 1$  modulation (the controller is turned on at  $t = 250$  ms) and (b)  $2N + 1$  modulation (the circulating current control is always active).

The peak-to-peak circulating current ripple can be directly estimated from the generated OPP

$$\Delta i_{circ,max} = \frac{V_{lvl}^*}{2} \frac{\Delta t_{red,max}}{2L_{br}} \quad (5)$$

where  $\Delta t_{red,max}$  is the maximum duration of a redundant level in the pattern. Note that this value depends on the modulation index  $m$ . It is important to emphasize that this high ripple is not visible in the three-phase grid currents.

Simulation results of the circulating current controller are illustrated in Fig. 8, highlighting its effectiveness for both  $N + 1$  and  $2N + 1$  modulation. It is noted that using these methods, the circulating current can be regulated along a reference trajectory with a certain amplitude and frequency. For additional details on the circulating current controllers, the reader is referred to the appendix.

### C. Interface to higher-level MMC inner voltage control

The proposed closed-loop-controlled OPPs and fast circulating current controllers can be interfaced in a straightforward manner to the higher-level MMC inner voltage control. This is shown in Fig. 9(a) for  $N + 1$  level modulation and in Fig. 9(b) for  $2N + 1$  level modulation.

The control block ‘MMC volt. ctrl’ controls the average converter dc-link voltage (total energy) by adjusting the three-phase power reference as needed. It also ensures that no imbalance occurs between the sums of the cell capacitor voltages in each branch. This is achieved by introducing appropriate circulating currents ( $i_{circ}^*$ ) with specific amplitudes and

frequencies, as widely described in the literature [15]–[18]. It is noted that other feed-forward terms can be also added to the circulating current references ( $i_{circ,ff}^*$ ) to achieve different purposes, such as capacitor voltage ripple minimization [19]–[21].

The control algorithm provides six switching patterns for each of the converter branches. These switching patterns are fed to the commonly used sort and selection algorithm, which determines the cell switching signals and balances the cell capacitor voltages within each branch.

## IV. PERFORMANCE EVALUATION

To evaluate the system performance, the converter control system with  $N + 1$  modulation was simulated using  $N = 8$  cells per branch and a semiconductor switching frequency of  $f_{sw} = 50$  Hz. The grid frequency is also 50 Hz. The OPP shown in Fig. 2 was computed, which minimizes the converter voltage TDD.

### A. Performance during transients

Despite the low apparent branch switching frequency, the control strategy offers a very good performance during transients. A three-phase power step is tracked within a few milliseconds, as shown in Fig. 10. This is achieved by manipulating the switching instants, thus adding or removing volt-second to the virtual converter flux. The branch capacitor voltage sums are quickly rebalanced after the transient, while the sorting and selection algorithm ensures equal voltage

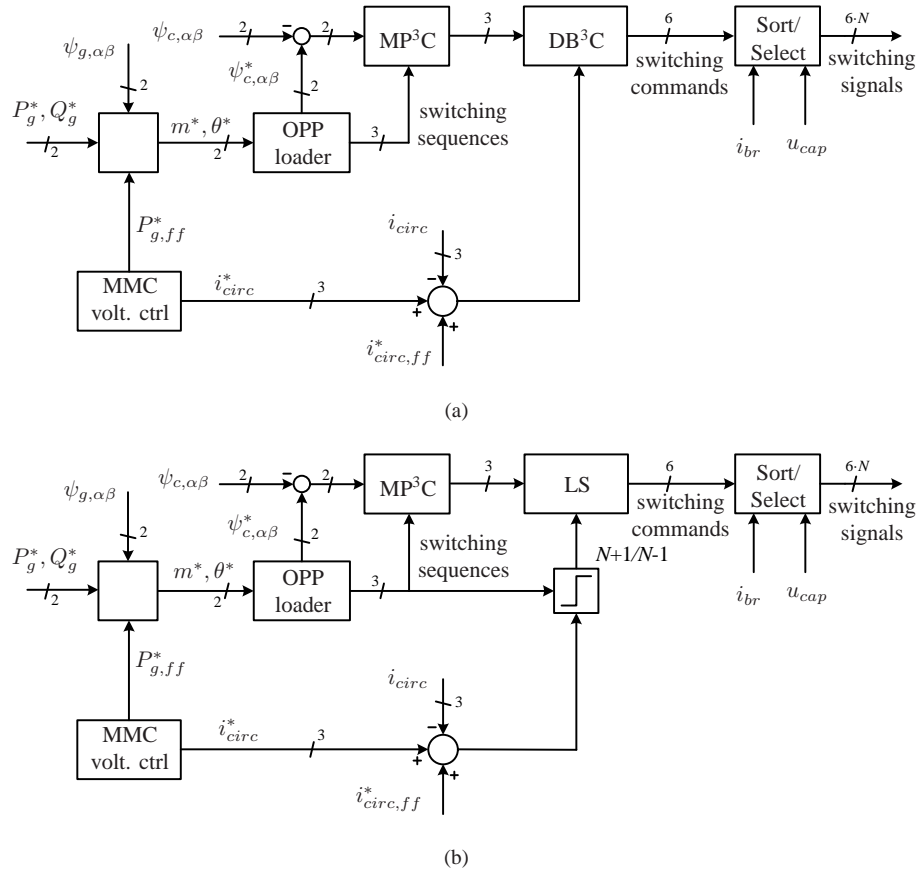


Fig. 9. Overall dc/ac MMC MP<sup>3</sup>C control diagram featuring the interface to the upper layer MMC inner voltage control as well as, (a) dead-beat circulating current control (DBC<sup>3</sup>) with  $N + 1$  modulation, (b) hysteresis circulating current control with  $2N + 1$  modulation.

distribution between the cells of the same branch. The performance could be even further improved with the pulse insertion method [22]. If a slower response were desired, the reference could be changed in a ramped rather than a step-wise manner.

Fig. 11 shows simulation results when changing the reference for the average converter cell voltage. This reference is first increased by 2% and then set back to its nominal value 100 ms later. The results highlight that the proposed control scheme is capable of controlling the average converter cell voltage. It also shows that the cell capacitor voltages can be chosen independently from the dc-link voltage. However, the circulating current features a higher ripple when the mismatch between the branch and dc-link voltages increases and when operating at such a low switching frequency and therefore reduced number of time instants when the circulating current control is active.

### B. Steady-state performance

Figure 12 illustrates the differential-mode line voltage spectrum for the case of  $N + 1$  modulation. The colours blue, green and red correspond to the phases  $a$ ,  $b$  and  $c$ . The OPP was chosen so as to minimize the voltage TDD. The results in Fig. 12 show a very discrete spectrum without even harmonics and interharmonics. In the specific example, no restrictions were imposed on specific harmonics. As a result, low-order harmonics, such as the 7<sup>th</sup> and 11<sup>th</sup> harmonics do appear, for

which the relevant grid standards normally allow for a higher amplitude.

Nevertheless, it might be beneficial to avoid such low-order harmonics, particularly when they are close to the frequencies of grid-side resonances. Depending on the degree of freedom, i.e., the pulse number  $d$ , several harmonics can be limited or even canceled. This is clearly shown in Fig. 13 for an  $N+1$  modulation, where the voltage TDD has been minimized while imposing soft constraints on the 7<sup>th</sup> and 11<sup>th</sup> harmonics using specific weighting factors. The harmonic energy is either placed in triplen harmonics, which are canceled out on a line voltage level, or it is moved to higher frequencies, thus simplifying the design of a grid filter.

### C. Comparison with flux tolerance band (FTB) modulation

At low cell numbers and switching frequencies, hysteresis-based control methods tend to outperform carrier-based ones. Therefore, for a comparative evaluation, the same system and operating point has been simulated using a modulation algorithm that keeps the virtual converter branch flux between predefined tolerance bands, similar to the one proposed in [23] for high-voltage dc (HVDC) MMC applications. The switching frequency of this flux tolerance band (FTB) controller is not constant, but it is adjusted indirectly in a trial-and-error procedure by choosing the tolerance band. To ensure a fair comparison with MP<sup>3</sup>C, the tolerance band was tuned such

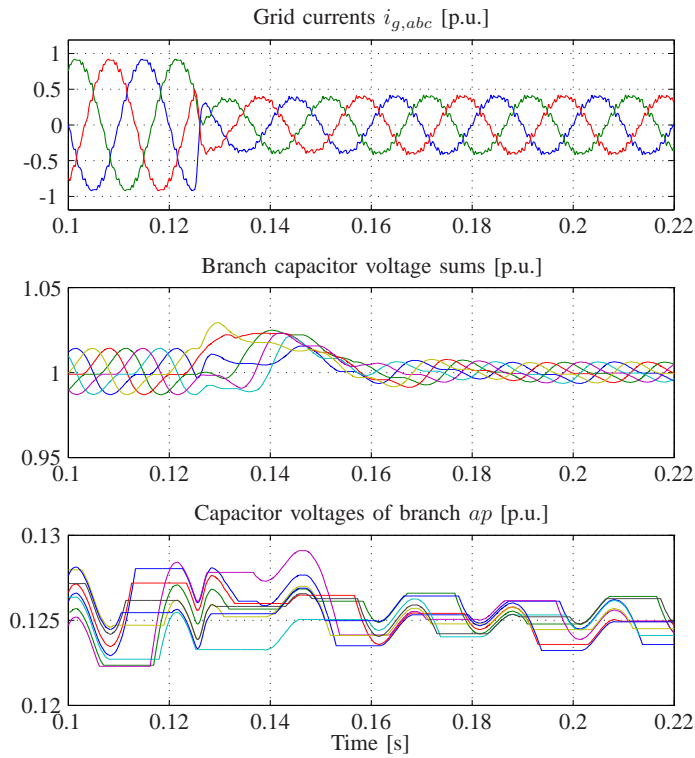


Fig. 10. Simulation results for an  $(N + 1)$ -modulated MMC during an active power reversal from  $P_g^* = 1$  p.u. to  $P_g^* = -0.5$  p.u. The middle graph illustrates the sums of capacitor voltages within each of the six converter branches whereas the bottom graph depicts the eight individual cell capacitor voltages within one converter branch.

that the same semiconductor switching frequency resulted as with MP<sup>3</sup>C, i.e.  $f_{sw} = 50$  Hz.

The simulation results of the FTB controller are shown in Fig. 14. A stochastic and wide voltage spectrum results, which is an inherent property of such a hysteresis-based method. The harmonic spectrum includes significant low-order harmonic energy, even harmonics and interharmonics. Moreover, the harmonic voltage spectrum differs between the three converter phases—as before, the colours blue, green and red correspond to the phases  $a$ ,  $b$  and  $c$ . This stands in contrast to the OPP method, for which the voltage harmonics in the three converter phases almost perfectly coincide, see Fig. 13(b).

## V. CONCLUSION

This paper proposed a fast closed-loop controller that allows the application of OPPs with discontinuous switching angles to a dc/ac three-phase MMC. This controller is a variation of the MP<sup>3</sup>C concept, and achieves a high controller bandwidth by directly manipulating the switching instants of the OPP. In a first step, the switching pattern is mapped to the upper and lower branches of each phase-leg, while performing grid-side virtual flux control. In a second step, circulating current control is accomplished for both  $N + 1$  and  $2N + 1$  modulation, which utilizes all converter degrees of freedom and makes this method compatible with the converter's upper layer voltage balancing controller.

The performance of the controller was evaluated during transients through power and voltage steps. During steady-

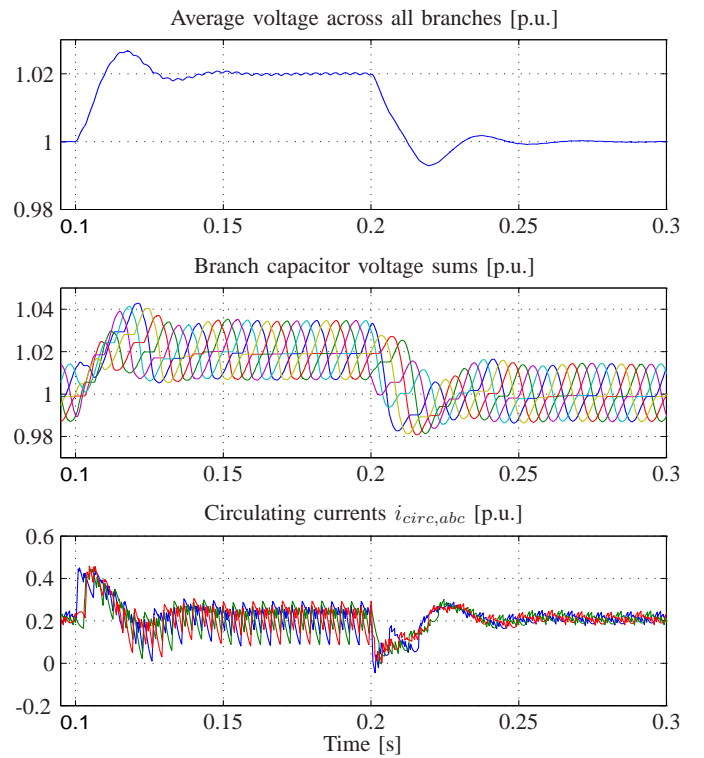


Fig. 11. Simulation results for an  $(N + 1)$ -modulated MMC during an increase of the total converter dc voltage from 1 to 1.02 p.u. at  $t = 0.1$  s. The dc voltage is reduced back to 1 p.u. at  $t = 0.2$  s.

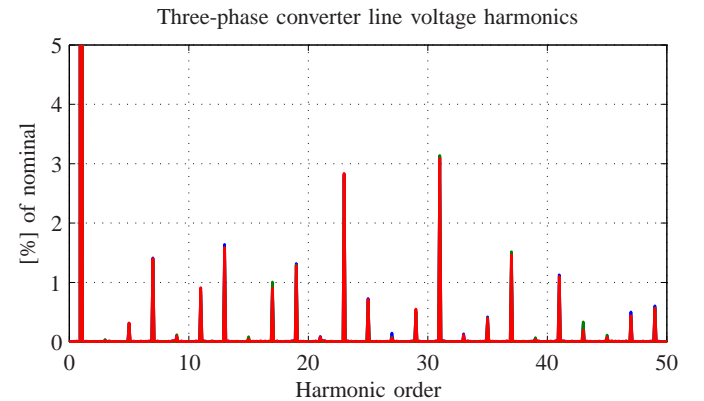


Fig. 12. Line voltage spectrum for the proposed MP<sup>3</sup>C controller with  $N + 1$  modulation and pulse number  $d = 4$ .

state operation, the comparison with an existing modulation method shows clear and significant advantages in terms of harmonic performance. Despite significant capacitor voltage ripples, the proposed control method preserves optimality of the pre-calculated pulse patterns in terms of their harmonic distortions. In summary, it was shown that OPPs provide a promising way to modulate medium voltage MMCs with low cell numbers when operating at low switching frequencies.

## APPENDIX

### SPECIAL CIRCULATING CURRENT CONTROL CASES

When combining MP<sup>3</sup>C with circulating current control, three cases might arise, which require particular attention in an implementation.

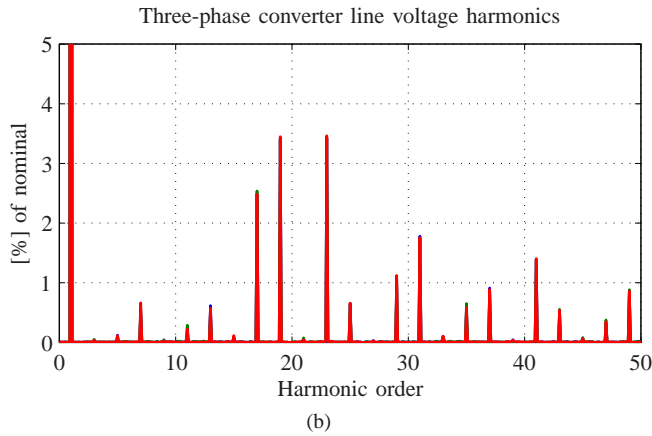
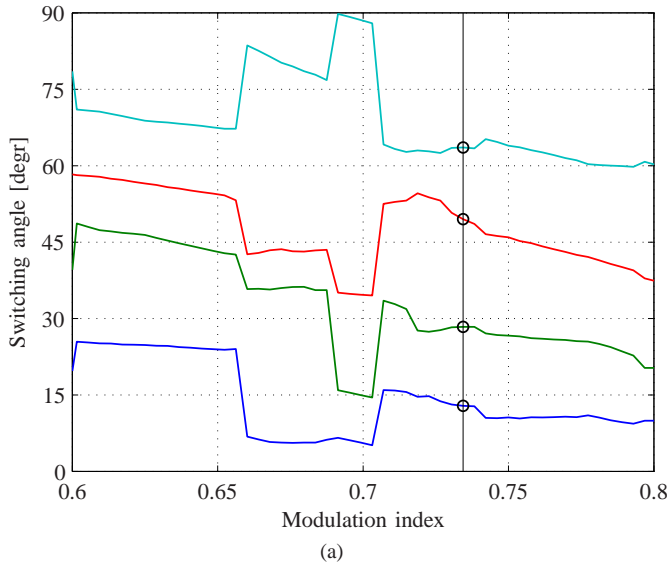


Fig. 13. (a) OPP switching angles and (b) line voltage spectrum for the proposed MP<sup>3</sup>C controller with  $N + 1$  modulation, pulse number  $d = 4$  and reduced low-order harmonics.

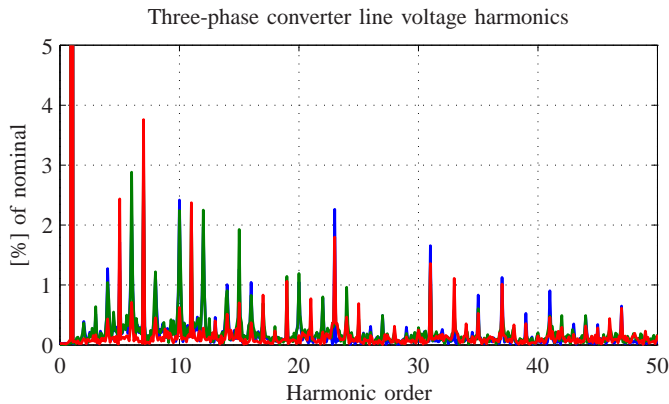


Fig. 14. Line voltage spectrum for flux tolerance band modulation and the same number of cells and switching frequency as in Fig. 12.

#### A. $N + 1$ modulation

In the first case, a switching transition originally occurring in the current sampling interval  $[t, t + T_s]$  is delayed until the next sampling interval in one of the two branches. To prevent the loss of the switching transition and an undesirable

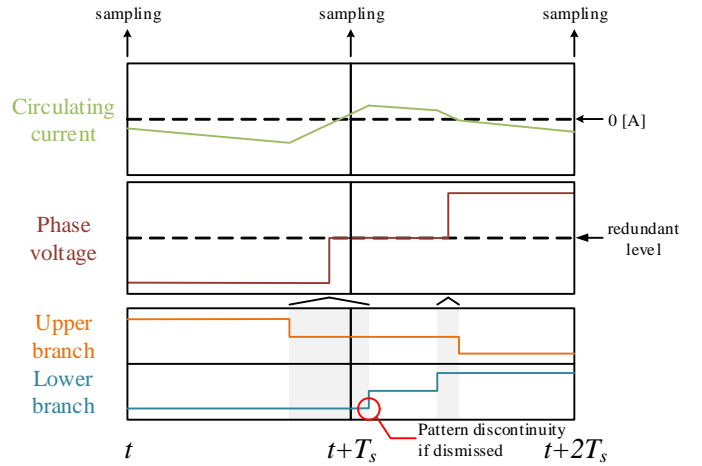


Fig. 15. Special case arising from the circulating current control with  $N + 1$  modulation: the switching transition in the current sampling interval is delayed to the next one.

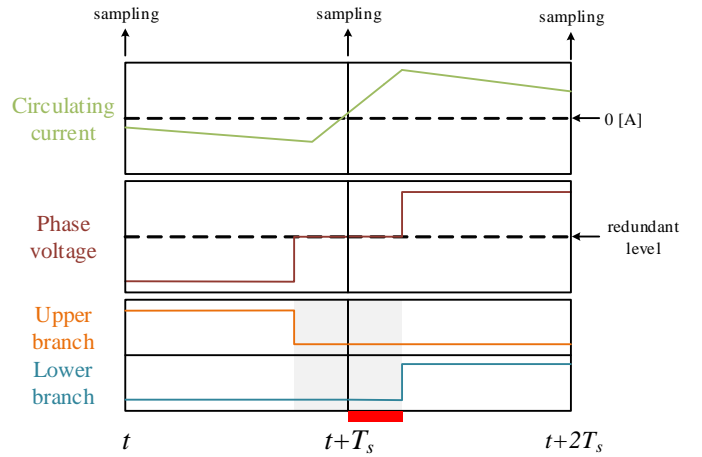


Fig. 16. Redundant level lock (red rectangle) in  $2N + 1$  modulation. The level lock is enabled at the end of the current sampling interval because of the sign change of the circulating current.

discontinuity in the phase switching pattern, a memory element should be added, which stores the transition until it is applied in the next sampling interval. This case is illustrated in Fig. 15.

In a second case, conversely, a switching transition originally occurring in  $[t + T_s, t + 2T_s]$  might be shifted to the current sampling interval in one of the two branches. A memory element is required to store the transition until it is applied in the other branch. In addition, the original switching transition in the phase cannot be modified anymore by MP<sup>3</sup>C for flux control.

#### B. $2N + 1$ modulation

The sign of the circulating current error may change between the two consecutive sampling intervals  $[t, t + T_s]$  and  $[t + T_s, t + 2T_s]$ , see Fig. 16. Ideally, the applied redundant level should be modified accordingly (i.e.  $N + 1 \leftrightarrow N - 1$ ), but this would increase the switching frequency. To prevent this, the applied redundant level should be locked in until a non-redundant level is applied.

## REFERENCES

- [1] A. Lesnicar and R. Marquardt, "A new modular voltage source inverter topology," in *Proc. 10th Eur. Conf. Power Electron. Appl.*, Toulouse, France, Sept. 2-4, 2003.
- [2] M. A. Perez, S. Bernet, J. Rodriguez, and S. Kouro, "Circuit topologies, modeling, control schemes and applications of modular multilevel converters," *IEEE Trans. Power Electron.*, vol. 30, no. 1, pp. 4-17, Jan. 2015.
- [3] G. S. Buja, "Optimum output waveforms in PWM inverters," *IEEE Trans. Ind. Appl.*, vol. 16, no. 6, pp. 830-836, Nov.-Dec. 1980.
- [4] K. Ilves, A. Antonopoulos, S. Norrga, and H.-P. Nee, "A new modulation method for the modular multilevel converter allowing fundamental switching frequency," *IEEE Trans. Power Electron.*, vol. 27, no. 8, pp. 3482-3494, Aug. 2012.
- [5] K. Ilves, A. Antonopoulos, L. Harnefors, S. Norrga, and H.-P. Nee, "Circulating current control in modular multilevel converters with fundamental switching frequency," in *Proc. 7th Int. Power Electron. Motion Control Conf. (ECCE Asia)*, pp. 249-256, June 2-5, 2012.
- [6] J. E. Huber and A. J. Korn, "Optimized pulse pattern modulation for modular multilevel converter high-speed drive," in *Proc. 15th Int. Power Electron. Motion Control Conf. (EPE-PEMC)*, pp. LS1a-1.4-1 - LS1a-1.4-7, Sept. 4-6, 2012.
- [7] G. Konstantinou, M. Ciobotaru, and V. G. Agelidis, "Selective harmonic elimination pulse-width modulation of modular multilevel converters," *IET Power Electron.*, vol. 6, no. 1, pp. 96-107, Jan. 2013.
- [8] G. Konstantinou, J. Pou, S. Ceballos, R. Picas, J. Zaragoza, and V. G. Agelidis, "Control of circulating currents in modular multilevel converters through redundant voltage levels," *IEEE Trans. Power Electron.*, vol. 31, no. 11, pp. 7761-7769, Nov. 2016.
- [9] A. Perez-Basante, S. Ceballos, G. Konstantinou, J. Pou, J. Andreu, and I. Martinez de Alegria, " $(2N+1)$  selective harmonic elimination-PWM for modular multilevel converters: A generalized formulation and a circulating current control method," *IEEE Trans. Power Electron.*, vol. 33, no. 1, pp. 802-818, Jan. 2018.
- [10] A. Edpuganti and A. K. Rathore, "Optimal pulsewidth modulation of medium-voltage modular multilevel converter," *IEEE Trans. Ind. Appl.*, vol. 52, no. 4, pp. 3435-3442, July-Aug. 2016.
- [11] A. Edpuganti and A. K. Rathore, "Optimal pulsewidth modulation for common-mode voltage elimination scheme of medium-voltage modular multilevel converter-fed open-end stator winding induction motor drives," *IEEE Trans. Ind. Electron.*, vol. 64, no. 1, pp. 848-856, Jan. 2017.
- [12] T. Geyer, N. Oikonomou, G. Papafiotou, and F. D. Kieferndorf, "Model predictive pulse pattern control," *IEEE Trans. Ind. Appl.*, vol. 48, no. 2, pp. 663-676, Mar./Apr. 2012.
- [13] V. Spudić and T. Geyer, "Fast control of a modular multilevel converter STATCOM using optimized pulse patterns," in *Proc. Energy Conv. Cong. Expo. (ECCE)*, pp. 1-8, Oct. 1-5, 2017.
- [14] M. Vasiladiotis, A. Christe, T. Geyer, and A. Faulstich, "Decoupled modulation concept for three-to-single-phase direct ac/ac modular multilevel converters for railway interties," in *Proc. Eur. Conf. Power Electron. Appl. (EPE)*, pp. 1-9, Oct. Sept. 11-14, 2017.
- [15] M. Hagiwara, R. Maeda, and H. Akagi, "Control and analysis of the modular multilevel cascade converter based on double-star chopper-cells (MMCC-DSCC)," *IEEE Trans. Power Electron.*, vol. 26, no. 6, pp. 1649-1658, June 2011.
- [16] J. Kolb, F. Kammerer, M. Gommeringer, and M. Braun, "Cascaded control system of the modular multilevel converter for feeding variable-speed drives," *IEEE Trans. Power Electron.*, vol. 30, no. 1, pp. 349-357, Jan. 2015.
- [17] P. Munch, D. Gorges, M. Izak, and S. Liu, "Integrated current control, energy control and energy balancing of modular multilevel converters," in *Proc. 36th IEEE Annu. Conf. Ind. Electron. Soc.*, pp. 150-155, Nov. 7-10, 2010.
- [18] A. Christe and D. Dujic, "Modular multilevel converter control methods performance benchmark for medium voltage applications," *IEEE Trans. Power Electron.*, vol. PP, no. 99, pp. 1-1, 2018.
- [19] M. Vasiladiotis, N. Cherif, and A. Rufer, "Accurate capacitor voltage ripple estimation and current control considerations for grid-connected modular multilevel converters," *IEEE Trans. Power Electron.*, vol. 29, no. 9, pp. 4568-4579, Sept. 2014.
- [20] M. Winkelkemper, A. Korn, and P. Steimer, "A modular direct converter for transformerless rail interties," in *Proc. IEEE Int. Symp. Ind. Electron.*, pp. 562-567, July 4-7, 2010.
- [21] J. Pou, S. Ceballos, G. Konstantinou, V.G. Agelidis, R. Picas, and J. Zaragoza, "Circulating current injection methods based on instantaneous information for the modular multilevel converter," *IEEE Trans. Ind. Electron.*, vol. 62, no. 2, pp. 777-788, Feb. 2015.
- [22] T. Geyer and N. Oikonomou, "Model predictive pulse pattern control with very fast transient responses," in *Proc. Energy Conv. Cong. Expo. (ECCE)*, pp. 5518-5524, Sept. 14-18, 2014.
- [23] A. Hassanpoor, L. Angquist, S. Norrga, K. Ilves, and H.-P. Nee, "Tolerance band modulation methods for modular multilevel converters," *IEEE Trans. Power Electron.*, vol. 30, no. 1, pp. 311-326, Jan. 2015.



grid-connected applications.

**Michail Vasiladiotis** (S'09-M'14) received the Diploma in electrical and computer engineering from the National Technical University of Athens (NTUA), Athens, Greece, in 2009, and the PhD degree from the the École Polytechnique Fédérale de Lausanne (EPFL), Lausanne, Switzerland, in 2014. Since 2015, he is with ABB Switzerland Ltd, Turgi, Switzerland, where he is currently working as a Senior R&D engineer on the product development of medium voltage high power multilevel static frequency converters for



control and modulation of multilevel converters for medium voltage applications.

**Alexandre Christe** (S'14) received the B.Sc., M.Sc. and PhD degrees in electrical engineering from the École Polytechnique Fédérale de Lausanne (EPFL), Lausanne, Switzerland, in 2012, 2014 and 2018, respectively.

From April 2014 till March 2018, he was with the Power Electronics Laboratory as a doctoral assistant. In May 2018, he joined ABB Corporate Research Center, Västerås, Sweden, as a Scientist.

His research interests include the design, control and modulation of multilevel converters for medium voltage applications.



currently a Senior Principal Scientist for power conversion control. He was appointed as an extraordinary Professor at Stellenbosch University, Stellenbosch, South Africa, from 2017 to 2020.

He is the author of more than 120 peer-reviewed publications, 30 patent applications, and the book "Model predictive control of high power converters and industrial drives" (Wiley, 2016). He teaches a regular course on model predictive control at ETH Zurich. His research interests include model predictive control, medium-voltage drives and utility-scale power converters.

Dr. Geyer is the recipient of four prize paper awards, including the 2017 First Place Prize Paper Award in the Transactions on Power Electronics. He served as an Associate Editor for the Transactions on Industry Applications. Since 2013 he has been serving as an Associate Editor for the Transactions on Power Electronics.